DIFFUSION WAVE MODELING OF DISTRIBUTED CATCHMENT DYNAMICS

By Stefano Orlandini[1] and Renzo Rosso[2]

ABSTRACT: A diffusion wave model of distributed catchment dynamics is presented. The effects of catchment topography and river network structure on storm-flow response are incorporated by routing surface runoff in cascade throughout a digital elevation model (DEM) based conceptual transport network, where the Muskingum-Cunge scheme with variable parameters is used to describe surface runoff dynamics. Dynamic scaling of hydraulic geometry is also incorporated in the model by using the "at-a-station" and "downstream" relationships by Leopold and Maddock. Numerical experiments indicate that the model is more than 98% mass conservative for possible slope and roughness configurations, which may occur for hillslopes in a natural catchment. Fluctuations in the simulated discharge may occur in response to discontinuities in rainfall excess representation if Courant number Cu during the simulation exceeds a threshold of about 3. Catchment scale simulations with different temporal resolution show that the model response is independent of structural parameters (model consistency). Also, the overall accuracy is preserved for computationally inexpensive space-time discretizations (for which $Cu > 3$) because fluctuations that may occur at the local scale are dampened when propagating downstream. Comparison of model results with observed outlet hydrographs of the Rio Missiaga experimental catchment (Eastern Italian Alps) show this approach to be capable of describing both overland and channel phases of surface runoff in mountainous catchments.

INTRODUCTION

Recent advances in remote sensing, geographic information systems, and computer technology make the use of distributed hydrologic models an attractive approach to flow simulation and prediction. The linkage of a distributed hydrologic model with the spatial data handling capabilities of digital elevation models (DEMs) and digital terrain models (DTMs) offers advantages associated with the full utilization of spatially distributed data to analyze hydrologic processes. The major areas of application of distributed models are in forecasting the effects of land-use change, the effects of spatially variable inputs and outputs, the movement of pollutants and sediments, and the hydrologic response of ungauged catchments (Beven and O'Connell 1982).

Surface runoff constitutes an important component of the hydrologic response of a catchment to climate and land use. A pioneering approach to the physical modeling of surface runoff was initiated by the simplified model of a catchment idealized by an open-book geometry (Wooding 1966). Also, numerical schemes to solve the governing equations of the physical processes have been given increasing importance, both for overland flows (Kibler and Woolhiser 1972; Ross et al. 1979; Brandford and Meadows 1990) and for channel flows (Szymkiewicz 1991). Despite the abundance of modeling schemes, the computational resources needed to run detailed models may be excessive for large-scale catchment simulations; hence there is a need for simpler conceptual techniques, which embody the essential concepts of component subprocesses while also allowing space-time variability to be considered.

Using the geomorphological-dispersion approach Rinaldo et al. (1991) found that in channel networks the dispersive character of the transport processes is determined by geometry and topology rather than the dispersive processes dominant at the mesoscale and microscale. Transport processes, from microscale to basin scales, experience spreading mechanisms from molecular to geomorphological diffusion in which the full development of any transition overwhelms the previous ones. This indicates that models based on accurate description of the geometry and topology of the river network and a simplified dynamics can capture the features of travel time distributions in a broad range of dispersivities.

In this paper a simple and computationally inexpensive model for distributed catchment dynamics is developed. The control of downslope water movement by catchment topography and channel network topology is treated by processing each of the DEM cells, from upland areas to the basin outlet, through a conceptual transport network extracted from DEM data. Each elemental network channel is assumed to have bed slope and length that depend on location within the DEM-extracted transport network, and rectangular cross section whose width varies dynamically according to the scaling properties of stream geometry as described by the "at-a-station" and "downstream" relationships first introduced by Leopold and Maddock (1953). Distinction between overland and channel flow is based on the "constant critical support area" concept [see Montgomery and Foufoula-Georgiou (1993)]. The use of grid-based DEMs instead of vector elevation data [see Moore and Grayson (1991)] is motivated by a series of interacting factors. On one hand, grid-based digital models are simple to use and elaborate and are still the more widespread support available for applications in operational hydrology. On the other hand, for large-scale catchment simulations, the dynamic scaling of channel geometry (see section titled "Channel Network Geometry") on a quasi-two-dimensional network extracted from grid-based data allows a physically realistic description of surface flow phenomena without incurring more complicated (and not always physically realistic) two-dimensional sheet flow representations.

A Muskingum-Cunge method with variable parameters is applied to control the amount of numerical diffusion in such a way that it matches the diffusion of the physical problem. The reliability and robustness of the routing model in terms of mass conservation, accuracy, and consistency are investigated through numerical experiments for a wide range of possible configurations of basin hillslopes (see section titled "Numerical Experiments at Hillslope Scale"). Model application to the 4.35-km^2 Rio Missiaga catchment (Eastern Italian Alps) shows that, even for computationally inexpensive space-time discretizations, mass conservation, accuracy, and consistency are significantly preserved (see section titled "Catchment

[1]Dr., DIIAR, Politecnico di Milano, Piazza Leonardo da Vinci, 32, Milano 20133, Italy. (e-mail: stefano@idra1.iar.polimi.it)

[2]Prof., DIIAR, Politecnico di Milano, Piazza Leonardo da Vinci, 32, Milano 20133, Italy. (e-mail: rr@idra1.iar.polimi.it)

Note. Discussion open until December 1, 1996. To extend the closing date one month, a written request must be filed with the ASCE Manager of Journals. The manuscript for this paper was submitted for review and possible publication on November 1, 1995. This paper is part of the ***Journal of Hydrologic Engineering***, Vol. 1, No. 3, July, 1996. ©ASCE, ISSN 1084-0699/96/0003-0103–0113/$4.00 + $.50 per page. Paper No. 11936.

Scale Modeling''). Finally, as an example of model application for investigative purposes, Eulerian and Lagrangian analysis of a Rio Missiaga catchment flood event is presented. Future work will consider large-scale catchment simulations to further test the capability of the model to reproduce the distributed flood dynamics and investigate the space-time variability of flow characteristics throughout the basin.

MODEL DESCRIPTION

Local contributions to infiltration excess runoff produced by the time compression approximation (TCA) model described in Orlandini et al. (in press, 1996) are routed onto a DEM-based conceptual transport network via a Muskingum-Cunge scheme with variable parameters. Surface runoff is not allowed to infiltrate in downslope cells even when the soil profile of these cells is not saturated. The runoff-runon problem is likely to be important where broad sheet flow occurs but relatively unimportant when the flow concentrates in defined rills, channels, and streams, as assumed in this model. There are two main aspects of the routing model presented in this work. The first aspect concerns the description of a watershed in terms of hydrologic features; the second concerns the representation of the flood wave phenomena that significantly characterize the catchment dynamics. These aspects are described in the following two sections, respectively.

Channel Network Geometry

The drainage network for a given catchment is automatically extracted from the DEM. Each grid cell is characterized by a maximum-slope pointer, and the network links are organized into a stream-ordering system extracted from the DEM data (Band 1986). Ordering is defined by assigning to each cell two numbers: the cell order and a link number. The first is the sum of the orders of the neighboring upslope cells from which the cell can receive water; source cells are assigned order 1. The link number identifies the first cell of each link in the network (Orlandini 1995). Distinction between overland and channel flow is based on the ''threshold drainage area concept'' as described in Montgomery and Foufoula-Georgiou (1993). This is shown in Fig. 1 with reference to the Rio Missiaga catchment application reported in a later section. A single formulation is used to describe the hydraulic geometry of the channel network for both overland and channel flow phenomena, but different parameter values can be taken to characterize cells in which overland or channel flow is assumed to occur.

Runoff over hillslopes or agricultural watersheds initially starts as sheet flow, then it concentrates into a series of small channels. The flow concentrations are due to either topographic irregularities or differences in soil erodibility. As runoff continues, erosion progresses and the channels deepen and widen as a function of slope steepness, runoff characteristics, and soil erodibility. Such erosion-formed microchannels are called rills or rivulets (Emmett 1978; Li et al. 1980). To minimize the computational effort and economize on the number of model parameters, in the model presented here the rill formations are lumped at the DEM elemental scale into a single conceptual wide channel with bed slope and geometry depending on DEM cell location and flow characteristics.

The elemental channels of the network are taken as wide rectangular channels with width depending on upstream drainage area and flow discharge. According to Leopold and Maddock (1953), if one considers discharge of various frequencies Q at a point of the river network, the flow width B scales with Q as

$$B = a'Q^{b'} \tag{1}$$

where the proportionality constant a' depends on the location of that point and the exponent b' is a characteristic of the channel network as a whole. When considering discharge with the same frequency, Q_r, at different points moving downstream in the basin the corresponding channel width B_r is given by

$$B_r = a''Q_r^{b''} \tag{2}$$

where a'' and b'' = characteristics of the river network. Although this is not necessarily equivalent to considering discharge resulting from the same event at different points, it can be assumed as a reasonable indicator of what may occur in that situation (Bras 1990).

At-a-station and downstream relationships, (1) and (2), respectively, can be coupled into a single equation to represent the dynamics of flow width at any point of the channel network in response to a rainfall excess forcing event. From (1) one obtains, for a given point in the channel network

$$\frac{B}{B_r} = \left(\frac{Q}{Q_r}\right)^{b'} \tag{3}$$

where B_r and Q_r = values of flow width and discharge at that point as given by (2). Eq. (2) yields

$$\frac{B_r}{B_{ro}} = \left(\frac{Q_r}{Q_{ro}}\right)^{b''} \tag{4}$$

where B_{ro} and Q_{ro} = values of the flow width and discharge at the basin outlet, for the considered frequency. By coupling (3) and (4), one obtains

$$B = B_{ro}\left(\frac{Q_r}{Q_{ro}}\right)^{b''}\left(\frac{Q}{Q_r}\right)^{b'} \tag{5}$$

As discharges Q_r in the various reaches corresponding to an outflow Q_{ro} are not known, estimation from a geomorphological relation is necessary. Leopold et al. (1964) report a relationship of wide applicability as

$$Q_b \propto A^{0.75} \tag{6}$$

where Q_b = bank-full discharge; and A = drainage area. The exponent in (6) may be closer to unity for small watersheds, especially in humid climates. To economize on the number of model parameters, the exponent in (6) is assumed equal to unity and the value of Q_r at a point of the river network is expressed using the formula

$$Q_r = q_r A \tag{7}$$

where q_r = corresponding reference value for rainfall excess; and A = upstream drainage area. Future adjustments of this assumption may be easily incorporated in the context of the model structure. From (7) the following is obtained:

$$\frac{Q_r}{Q_{ro}} = \frac{A}{A_o} \tag{8}$$

where A_o = catchment area, which is substituted for Q_r/Q_{ro} in (5) to obtain

$$B = B_{ro}Q_{ro}^{-b'}\left(\frac{A}{A_o}\right)^{b''-b'}Q^{b'} \tag{9}$$

This can be written as

$$B = \mathcal{B}Q^{b'} \tag{10}$$

where $\mathcal{B}$ = constant depending on location of the point in the river network and is given by

$$\mathcal{B} = B_{ro}Q_{ro}^{-b'}(A/A_o)^{b''-b'} \tag{11}$$

The hydraulic geometry of the channels in the river network is lumped into a single parameter, that is, $B_{ro}Q_{ro}^{-b'}$. During a

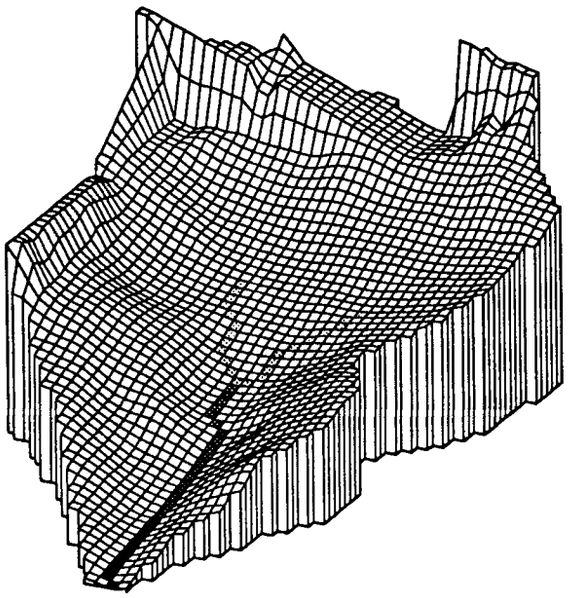

FIG. 1. 50 × 50 m² Resolution DEM of Rio Missiaga Experimental Catchment Showing Cells in Which Overland Flow (White Cells) and Channel Flow (Dark Cells) Occurs

flood the active channel width scales dynamically with discharge with the same exponent of the at-a-station relationship, and with the upstream basin area with an exponent equal to the difference of those of downstream and at-a-station relationships. If one lets Q_{ro} be equal to 1, B_{ro} is the only structural parameter of the channel network.

Eq. (10) can be applied to represent the network dynamics in response to a rainfall excess event. For $b' = 0$ hydraulic geometry varies in space but not in time, while for $b' > 0$ it varies both in space and time. This structure is used to describe both overland and channel flow. For all those catchment cells with upstream drainage area A less than a given threshold A^*, it is assumed that only overland flow occurs, whereas channel flow is assumed to occur in cells for which A exceeds A^*. This simple criterion for catchment cell classification is represented in Fig. 1 for the Rio Missiaga catchment, assuming $A^* = 0.50$ km^2. Different values of b', b'', and B_{ro} ($Q_{ro} = 1$) may be assumed to characterize overland and channel flow cells.

Diffusion Wave Formulation

The same routing scheme is applied for both overland and channel flow, but different distributions of the Gauckler-Strickler roughness coefficient may be considered to account for the different processes that characterize overland and channel flow. The routing model developed in this study is based on the Muskingum-Cunge method (Cunge 1969). This method is simple to formulate and use, and it allows physical damping of the flood wave to be artificially described through the numerical diffusion in the scheme (due to truncation errors). The model routes surface runoff downstream, link by link, from the uppermost cell in the basin to the outlet. A given grid cell will receive water from its upslope neighbors and discharge to its downslope neighbor according to the network ordering system described earlier. At any catchment cell the lateral inflow rate q_L (L^2T^{-1}) is given by

$$q_L = q\Delta x\Delta y/\Delta s \tag{12}$$

where q (LT^{-1}) = local contribution to infiltration excess runoff; Δx and Δy = DEM-cell sizes in the direction of the x and y horizontal coordinates; and Δs = channel length within the cell.

Inflow hydrographs and lateral inflows q_L are routed onto each individual channel via the routing equation

$$Q_{i+1}^{j+1} = C_1Q_i^{j+1} + C_2Q_i^j + C_3Q_{i+1}^j + C_4q_{Li+1}^{j+1} \tag{13}$$

where Q_{i+1}^{j+1} = discharge at network link point $(i + 1)\Delta s$ and time $(j + 1)\Delta t$; and q_{Li+1}^{j+1} = lateral inflow rate at the $(i + 1)$th space interval and $(j + 1)$th time interval (see Fig. 2). The routing coefficients, C_1, C_2, C_3, and C_4, are given by

$$C_1 = \frac{c_k(\Delta t/\Delta s) - 2X}{2(1 - X) + c_k(\Delta t/\Delta s)} \tag{14}$$

$$C_2 = \frac{c_k(\Delta t/\Delta s) + 2X}{2(1 - X) + c_k(\Delta t/\Delta s)} \tag{15}$$

$$C_3 = \frac{2(1 - X) - c_k(\Delta t/\Delta s)}{2(1 - X) + c_k(\Delta t/\Delta s)} \tag{16}$$

$$C_4 = \frac{2c_k\Delta t}{2(1 - X) + c_k(\Delta t/\Delta s)} \tag{17}$$

where c_k = kinematic wave celerity; and X = weighting factor used for discretizing the temporal derivative of the kinematic flow equation

$$\frac{\partial Q}{\partial t} + c_k\frac{\partial Q}{\partial s} = c_kq_L \tag{18}$$

X is used to match the numerical diffusion coefficient of the scheme

$$D_n = c_k\Delta s(1/2 - X) \tag{19}$$

and the hydraulic diffusivity D_h in the convection-diffusion flow equation

$$\frac{\partial Q}{\partial t} + c_k\frac{\partial Q}{\partial s} = D_h\frac{\partial^2 Q}{\partial s^2} + c_kq_L \tag{20}$$

If one incorporates (10) into the Manning-Gauckler-Strickler friction equation, (see Appendix I), one obtains

$$Q = \mathcal{B}^{-2/(3+2b')}k_S^{3/(3+2b')}S_f^{3/[2(3+2b')]}\Omega^{5/(3+2b')} \tag{21}$$

where k_S = apparent Gauckler-Strickler roughness coefficient; S_f = friction slope; and Ω = flow area (see Appendix I). For $b' = 0$ one has the case of channel with fixed width $\mathcal{B}$. The kinematic flood wave celerity $c_k = dQ/d\Omega$ is expressed by

$$c_k = 5/(3 + 2b')Q/\Omega \tag{22}$$

that expands into the expression

$$c_k = 5/(3 + 2b')\mathcal{B}^{-2/5}k_S^{3/5}S_0^{3/10}Q^{2/5(1-b')} \tag{23}$$

in which one has assumed $S_f = S_0$, where $S_0 = \sin\beta$ is the channel bed slope; and β = channel bed inclination angle (see Appendix I). The effect of the dynamic scaling of channel width with flow on the flood wave celerity is represented in Fig. 3 for a set of parameters taken as representative of channel flow for the Rio Missiaga catchment, by varying b' in (23).

From the friction equation (21), one obtains the following

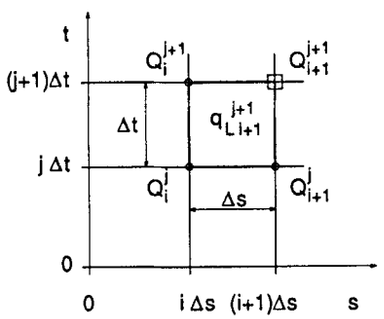

FIG. 2. Space-Time Computational Grid of Muskingum-Cunge Method

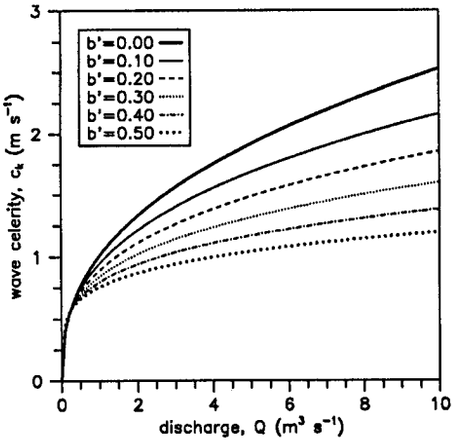

FIG. 3. Effect of Dynamic Scaling of Channel Width on Flood Wave Celerity c_k [Eq. (23)], for B_{ro} = 7 m (Q_{ro} = 1 m^3 s^{-1}), $A = A_o$, $b'' = 0.50$, k_s = 5 m$^{1/3}$ s^{-1}, and $S_0 = 0.10$

expression for the hydraulic diffusivity in the convection-diffusion equation (see Appendix I)

$$D_h = \frac{3Q^{1-b'} \cos \beta}{2(3 + 2b')\mathcal{B}S_0} \tag{24}$$

and thus, by matching D_n and D_h given by (19) and (24), respectively, the weighting factor X can be expressed as a function of channel and flow characteristics, that is

$$X = 1/2(1 - D) \tag{25}$$

where

$$D = \frac{3Q^{1-b'} \cos \beta}{(3 + 2b')\mathcal{B}S_0 c_k \Delta s} \tag{26}$$

Wave celerity c_k and weighting factor X are varied at each computational cell according to (23) and (25), in which discharge Q is estimated via a three-point average discharge $\bar{Q} = (Q_i^j + Q_{i+1}^j + Q_i^{j+1})/3$ (Ponce and Yevjevich 1978). By varying X with the flow the numerical diffusion coefficient D_n is used to simulate the hydraulic diffusivity D_h of the actual flood wave. For $X = 1/2$ there is no numerical diffusion. For $X > 1/2$ the numerical diffusion coefficient is negative and the numerical scheme is therefore unstable; however, such occurrence is avoided by matching numerical and physical diffusivities and this ensures the unconditional stability of the scheme. In the Muskingum-Cunge method, X is interpreted as a diffusion-matching factor and thus negative values of X are possible.

The Muskingum-Cunge method offers several advantages over the standard kinematic wave methods. First, the solution is obtained through a linear algebraic equation, (13), instead of a finite difference or characteristic approximation of a partial differential equation; this allows the entire hydrograph to be obtained at required cross section without solving over the entire length of the channel for each time step. Second, the solution using (13) will permit a more flexible choice of time and space increments in order to obtain accurate and stable computations as compared to the kinematic wave method. Finally, the diffusion method provides grid independence for a wide range of resolution levels, while the kinematic method does not (Ponce 1986).

Some of the disadvantages of the Muskingum-Cunge method are that it cannot handle downstream disturbances that propagate upstream, and that it does not accurately predict the discharge hydrograph at a downstream boundary when there are large variations in the kinematic wave speed, such as those that result from inundation of large floodplains (Natural 1975). Simulation of backwater effects in catchment dynamics can be used to allow flow over "digital dams" (due to errors in DEM data); for example, in the model presented by Julien et al. (1995), surface water accumulates behind the barrier until the depth exceeds the barrier height and then spills over. In the model presented here, "digital pits" are filled in a preprocessing step, before extracting the channel network from the catchment DEM, so that a certain degree of accuracy in the catchment topography representation is forfeited in exchange for simplicity and robustness in the flow dynamics description.

Numerical Experiments at Hillslope Scale

Numerical experiments over hypothetical hillslopes are performed in order to investigate mass conservation, accuracy, and consistency of the presented model. Analysis of the numerical scheme is carried out for the case $b' = 0$: this simplifies notation without too much loss of generality. In fact, numerical experience shows that the numerical behavior of the model is not very sensitive to b' and that $b' = 0$ represents the most severe condition. In the context of this study, accuracy refers to the avoidance of physically unrealistic outflows and fluctuations in discharge that may occur in response to discontinuities in rainfall excess representations. Consistency refers to the ability of the routing method to produce the same results regardless of grid size. This concept is to be used within the framework of a simplified routing method in which the objective is to optimize the numerical diffusion by matching the physical diffusion, and it should not be confused with the property of consistency of a conventional finite difference scheme, in which the objective is to minimize the amount of numerical error in order to properly solve the differential equation under consideration (Ponce and Theurer 1982).

The examined hillslope consists of 20 square cells with grid spacing Δx, arranged to form a single plane (Fig. 4). Hillslope response to a synthetic step function of rainfall excess is investigated over a range of rainfall excess rates q, grid spacings Δx, time-step resolutions Δt, mean slopes $\bar{S}_0$, Gauckler-Strickler roughness coefficients k_S, and channel widths at the outlet, B_{ro}. The base case parameter set for the runs and the parameter ranges investigated are reported in Table 1. Parameters q, Δx, Δt, $\bar{S}_0$, k_S, and B_{ro}, respectively, are varied, keeping all other parameters fixed.

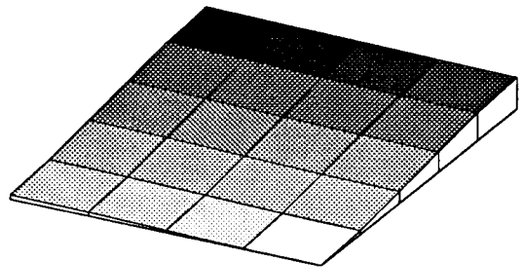

FIG. 4. DEM of Hypothetical Hillslope Used to Test Mass Conservation and Accuracy of Routing Scheme (Darker Shades Represent Higher Cell Elevations)

TABLE 1. Model Parameters for Hillslope Scale Tests

Parameter (1)	BCPS[a] (2)	Parameter ranges (3)
q, mm h^{-1}	10	1, 2, 3, 5, 10, 20
Δx, m	50	10, 20, 30, 50, 100, 200, 300, 500
Δt, h	1/12	1/240, 1/120, 1/60, 1/36, 1/24, 1/12, 1/6
$\bar{S}_0$	0.084	0.017, 0.084, 0.336
k_s, m$^{1/3}$ s^{-1}	10.0	0.7, 1.4, 2.8, 5.6, 10.0, 20.0, 40.0, 80.0
B_{ro}, m	2.0	0.5, 1.0, 2.0, 4.0, 8.0, 16.0

[a]Base case parameter set

Mass conservation is monitored by integrating the outflow hydrographs for all runs reported in Table 1. The relative mass balance errors are expressed as

$$\varepsilon_M = (V_Q - V_q)/V_q \tag{27}$$

where

$$V_q = \int_A \int_T q \, dA \, dt \tag{28}$$

is the cumulative volume of rainfall excess produced over the entire hillslope area A during the simulation period T, and

$$V_Q = \int_T Q \, dt \tag{29}$$

is the cumulative volume of outlet discharge Q during the simulation period T. Relative errors in mass balance are found to be less than 2% for all simulations.

To obtain an accurate solution of the Muskingum-Cunge method it is generally recommended to respect the empirical criterion

$$C_1 \geq 0 \tag{30}$$

whereas negative values for C_2 and C_3 do not affect the overall accuracy of the method (Ponce and Theurer 1982). Condition (30) is verified if, and only if,

$$Cu + D \geq 1 \tag{31}$$

where $Cu = c_k \Delta t/\Delta s$ is the Courant number; and $D = 1 - 2X$. For wide channels with rectangular cross sections, one has

$$Cu = 5/3B^{-2/5}k_S^{3/5}S_0^{3/10}(\Delta t/\Delta s)\bar{Q}^{2/5} \tag{32}$$

$$D = \frac{\bar{Q}^{3/5}\cos\beta}{5/3k_S^{3/5}S_0^{13/10}B^{3/5}\Delta s} \tag{33}$$

Thus, (30) can be expressed in terms of discharge as

$$Q \geq \left[\frac{5(1 - Cu)}{3\cos\beta} k_S^{3/5}S_0^{13/10}B^{3/5}\Delta s\right]^{5/3} \tag{34}$$

When overland flow is examined, (34) may not be attained, especially in upland areas. In this case the value of $\bar{Q}$ in (33) can be forced to meet (34), which is equivalent to the condition

$$D = 1 - Cu \tag{35}$$

for calculations of $X = 1/2(1 - D)$. This causes the numerical diffusion coefficient of the computational scheme to exceed the hydraulic diffusivity for small values of discharge. Computational results show that for the range of situations that may occur in a natural catchment, (35) improves the accuracy of the scheme without significantly changing the features of catchment response.

Since no general criteria for accuracy (in the sense specified previously) are available for the Muskingum-Cunge method with variable parameters, the results of numerical experiments are reported as an alternative indicator for accuracy and consistency. In the linear analysis of the scheme, the numerical dispersion is minimized when the Courant number is kept close to 1 (Cunge 1969). In the nonlinear case the Courant number is allowed to vary at each computational cell of Fig. 2; therefore, it is not possible to establish a priori whether the accuracy is preserved. Nevertheless, accuracy is still affected by the factors of (32), and the influence of these factors is related to the corresponding exponent. For instance, accuracy is affected by space and time resolution (order 1) more than by topographic slope (order 3/10). From the numerical experiments performed in this study, it is found that fluctuations occur when, in the computational domain, Courant numbers exceed a threshold value Cu^*; an estimate of Cu^* is 3. The hillslope response for the base case parameter set of Table 1 is shown in Fig. 5. Courant numbers during the simulation range from 0.59 to 4.73 and this produces fluctuations in discharge in response to the discontinuities in rainfall excess representation. The effect of the Courant number on numerical dispersion is empirically investigated by varying all the factors of (32) as reported in Table 1. For example, the effect of in-

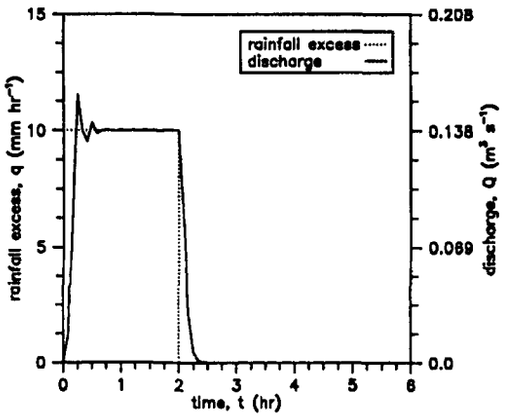

FIG. 5. Hillslope Response to Step Function of Rainfall Excess for Base Case Parameter Set of Table 1 (During Simulation, Courant Number *Cu* Ranges from 0.59 to 4.73)

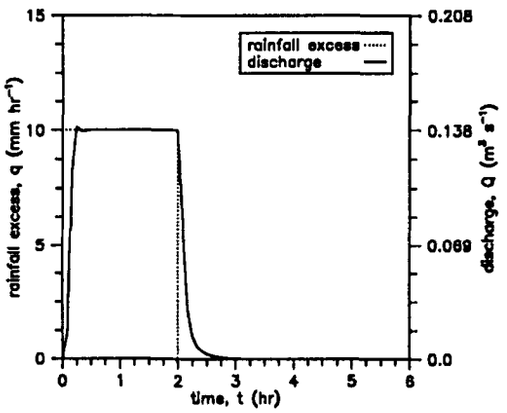

FIG. 6. Hillslope Response to Step Function of Rainfall Excess for Base Case Parameter Set of Table 1, Except with Δt = 1/24 h; Fluctuations in Discharge Evident in Fig. 5 Are Significantly Reduced (During Simulation, Courant Number *Cu* Ranges from 0.29 to 2.33)

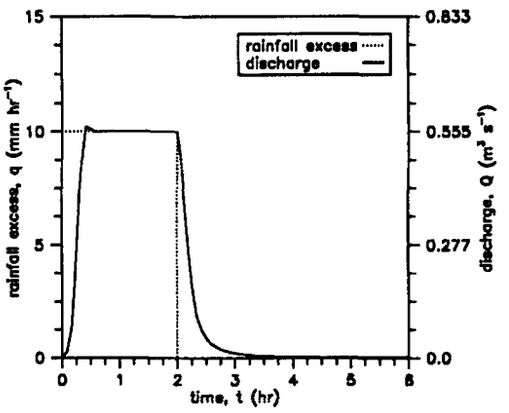

FIG. 7. Hillslope Response to Step Function of Rainfall Excess for Base Case Parameter Set of Table 1, Except with Δx = 100 m and B_w = 4 m (During Simulation, Courant Number *Cu* Ranges from 0.18 to 2.49)

creasing the time resolution (smaller Δt) is represented in Fig. 6. For the same set of parameters used for the run plotted in Fig. 5, except with Δt = 1/24 h, the Courant number ranges from 0.29 to 2.33. This caused numerical dispersion to be reduced and fluctuations in discharge to be significantly decreased. The same effect can be obtained by varying each of the factors in (32) so as to reduce the Courant number during the simulation. In particular, the effects of increasing the grid spacing Δx encourage the model application for large-scale catchment analysis (Fig. 7).

CATCHMENT SCALE MODELING

The network routing model described earlier was tested on the Rio Missiaga experimental catchment, located on the western side of the Cordevole Valley (Belluno, Italy). The catchment's main geological and geomorphological features are reported in Friz et al. (1983). A 4.35-km^2 extension of the Rio Missiaga catchment was horizontally discretized into 1,740 cells with a 50-m grid spacing (Δx = 50 m, see Fig. 1). The Rio Missiaga catchment ranges in elevation from 1,100 m above sea level at the outlet to more than 2,400 m above sea level. Identification of the channel network from the DEM of the catchment was carried out through the critical support area with constant threshold A^* = 0.50 km^2. This threshold value was selected on the basis of visual similarity between the extracted network and the blue lines depicted on topographic maps. Structural parameters of the drainage network and Gauckler-Strickler roughness are reported in Table 2. Exponents b' and b'' introduced earlier are assumed to be b' = 0.26 and b'' = 0.50, as found by Leopold and Maddock (1953) for the semiarid catchments of the United States. These exponent values provide flow widths that are in reasonable agreement with the hydraulic geometry of the catchment network, although more extensive field data must be collected in order to fit and verify relationships (1) and (2), and to conduct a comprehensive model calibration and parameter optimization.

Surface cover and soil properties are assigned to each DEM cell on the basis of the available information on catchment attributes and a TCA water balance model is applied to calculate rainfall excess at a 1-h time-step resolution. Complete details of the TCA water balance model formulation and parameterization are given by Orlandini et al. (in press, 1996). The nonuniform distribution of soil and vegetation parameters produces a distributed rainfall excess response of the catchment that is qualitatively in agreement with field observations. Infiltration excess is the dominant surface runoff production mechanism for lowland areas, where fine-grained sedimentation results in relatively low surface hydraulic conductivities, although strong subsurface kinematic storm-flow response from the coarse-grained upland areas can also occur during extreme storm events. The subsurface storm-flow response of the catchment is described in this study through the diffusion wave formulation outlined in Appendix II.

The apparent Gauckler-Strickler roughness coefficient k_S is the only (distributed) parameter of the routing model. For the Rio Missiaga catchment, uniform distributions for k_S are assumed and, as reported in Table 2, different values of k_S are considered for cells in which overland or channel flow is assumed to occur (see Fig. 1). This allows one to take into account the different dissipative processes that characterize overland and channel flow. Small values of k_S assumed to calibrate the model are in agreement with observed data reported in the literature. Kouwen and Li (1980) found, for flow through grass-lined channels, values of Manning roughness n = 0.05–0.5 m$^{-1/3}$ s (k_S = 2–20 m$^{1/3}$ s^{-1}). Newson and Harrison (1978) found that for sheet flow n = 25 m$^{-1/3}$ s (k_S = 0.04 m$^{1/3}$ s^{-1}). Bathurst (1986) used an intermediate value of Gauckler-Strickler roughness, k_S = 0.75 m$^{1/3}$ s^{-1} (n = 1.33 m$^{-1/3}$ s), to describe overland flow that occurs in rivulets, and this value is in agreement with the values derived from the data of Emmett (1978). The Gauckler-Strickler roughness coefficient used in the context of this study is to be assumed as an overall parameter to which many flow processes that occur in a natural hillslope may contribute. This may explain the small values of k_S required to describe flows in natural channels with respect to the case of artificial channels.

The model was calibrated using data for the flood event shown in Fig. 8. Model validation was then carried out using data for the events shown in Figs. 9 and 10, where calibration values of soil and channel network hydraulic properties are maintained; initial conditions of catchment wetness are estimated on the basis of precipitation prior to the simulation events. A 1-h time step is used for infiltration excess calculations and a 5-min time step (Δt = 1/12 h) is used to control the accuracy of the routing scheme. The calibration event shown in Fig. 8 is reproduced by the model simulation in both the infiltration excess and kinematic subsurface runoff components (see Appendix II). The rising limb and first peak of the hydrograph reflect surface runoff response, whereas successive peaks and the tail reflect kinematic subsurface storm-flow response. As shown in Figs. 9 and 10, the validation events are reasonably well simulated by the model. The hydrographs for the two validation events represent predominantly surface runoff response, as indicated by the single peaks of shorter duration and shorter tails.

As shown in Fig. 9, fluctuations in discharge that may occur at the elemental cell-channel scale for Δt = 1/12 h (see Fig. 5) are dampened when propagating downstream, and this explains why the outlet hydrographs do not significantly differ from the hydrographs obtained for extremely high temporal resolution, Δt = 1/60 h, for which fluctuations do not occur (see Fig. 6). The consistency of the method is also confirmed.

TABLE 2. Model Parameters for Rio Missiaga Catchment Simulations

Parameter (1)	Values	
	Overland flow (2)	Channel flow (3)
b'	0.26	0.26
b''	0.50	0.50
B_{ro}, m	25	7
Q_{ro}, m^3 s^{-1}	1	1
k_S,[a] m$^{1/3}$ s^{-1}	0.7	5.0

[a] $1/n$, where n is Manning's roughness.

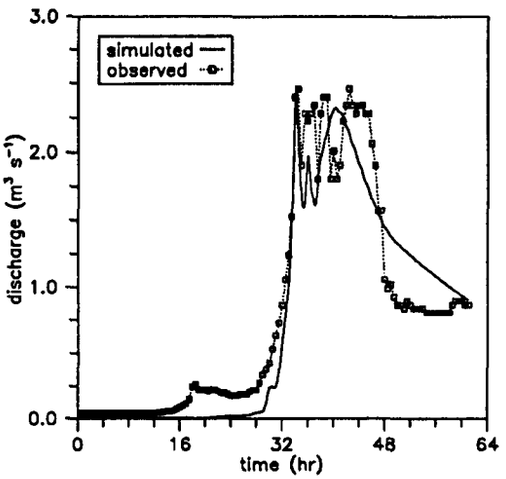

FIG. 8. Comparison between Simulated and Observed Outlet Storm Flow for October 9–12, 1987 Rio Missiaga Flood Calibration Event

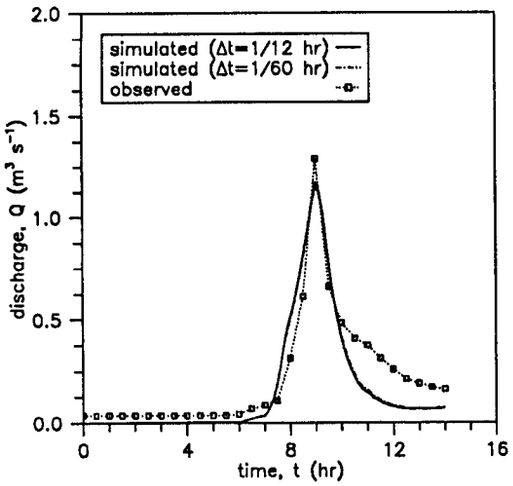

FIG. 9. Comparison between Simulated and Observed Outlet Storm Flow for September 29, 1991 Rio Missiaga Flood Validation Event

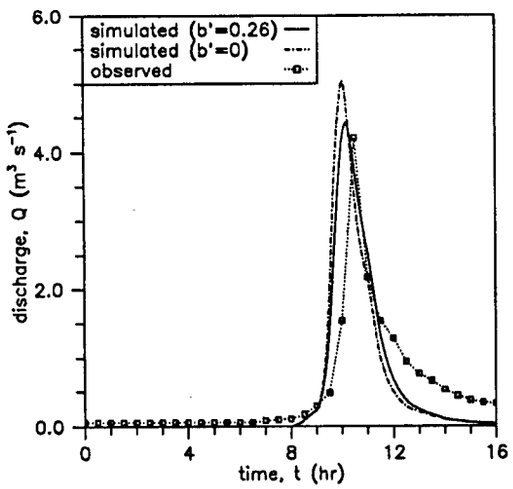

FIG. 10. Comparison between Simulated and Observed Outlet Storm Flow for September 14, 1993 Rio Missiaga Flood Validation Event

In Fig. 10 the effect of the dynamic scaling of flow width on the catchment response is investigated. As expected from (23) and Fig. 3, the change in wave celerity in the case of dynamically scaled flow width ($b' = 0.26$) produces a slower catchment response and a smaller hydrograph peak in comparison to the case of static flow width ($b' = 0$). This effect is enhanced when the discharge increases, and thus further investigations for larger scale catchment simulations are suggested.

As an example of model application for investigative purposes both Eulerian and Lagrangian analysis of the September 14, 1993 flood event are presented. The five locations A–E (channel sections) and the flow path shown in Fig. 11 are selected for the Eulerian and Lagrangian analysis, respectively. Some hydrologically relevant features along the selected path are reported in Table 3. As shown in Fig. 12, the Eulerian analysis of the flood event is carried out by plotting the surface runoff hydrographs at five locations along the path. The Lagrangian analysis of the flood event is carried out by plotting surface flow characteristics along the selected path, for four given instants in time. Flow discharges, depths, and velocities are shown in Figs. 13, 14, and 15, respectively. For the considered flood event, average velocities increase in a downslope direction along the path, and the rate of increase is qualitatively in agreement with published data [e.g., Carlston (1969), Pilgrim (1977)]. Therefore, one must properly account for this

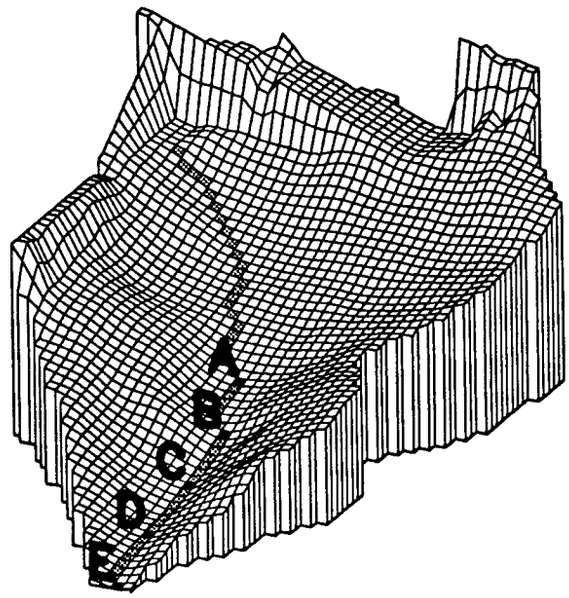

FIG. 11. DEM of Rio Missiaga Catchment Showing Selected Locations (Black Cells, A–E) and Path (Dark Cells) for Eulerian and Lagrangian Analysis of September 14, 1993 Flood Event

TABLE 3. Characteristics of Path Shown in Fig. 11 and Peak Discharges at Selected Locations[a]

Location (1)	s[b] (km) (2)	A (km²) (3)	$\mathcal{B}$[c] (m) (4)	$\mathcal{B}$[d] (m) (5)	Q_{peak} (m³ s⁻¹) (6)
A	1.450	1.3825	3.94	5.32	0.27
B	1.842	3.1125	5.92	6.46	1.10
C	2.192	3.4675	6.24	6.63	2.02
D	2.592	4.2000	6.87	6.94	3.77
E	3.062	4.3500	7.00	7.00	4.41

[a]Rio Missiaga September 14, 1993 flood event (see Fig. 10).
[b]Downstream spatial coordinate.
[c]Static description ($b' = 0$).
[d]Dynamic description ($b' = 0.26$).

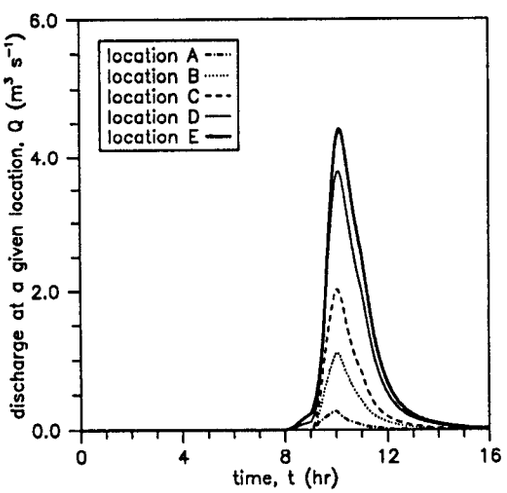

FIG. 12. Surface Runoff Hydrographs at Locations A–E Shown in Fig. 11, for September 14, 1993 Rio Missiaga Flood Event

variability when using the geomorphologic instantaneous unit hydrograph to model basin response [see Agnese et al. (1988)].

The effect of topography on catchment dynamics can be expressed in terms of the Péclet number. The Péclet number

$$Pe = 4UY/D_h \tag{36}$$

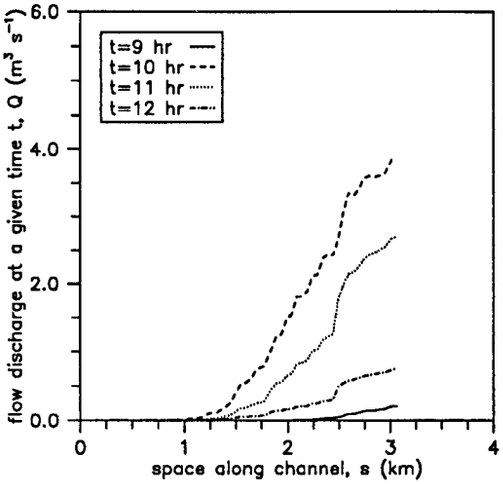

FIG. 13. Surface Runoff Discharge along Path Shown in Fig. 11, for Different Instants in Time of September 14, 1993 Rio Missiaga Flood Event

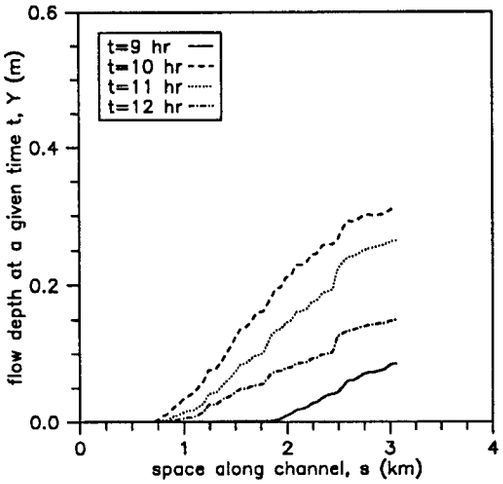

FIG. 14. Surface Runoff Depth along Path Shown in Fig. 11, for Different Instants in Time of September 14, 1993 Rio Missiaga Flood Event

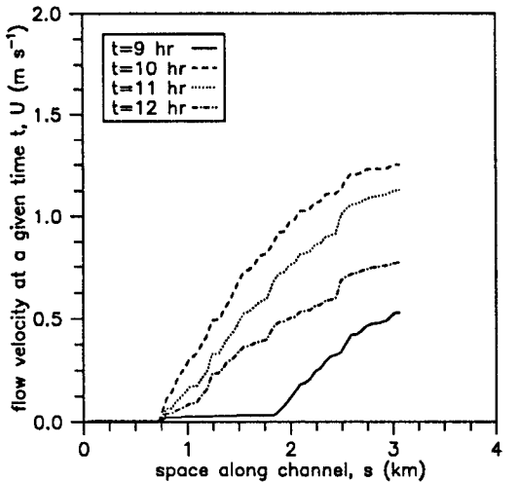

FIG. 15. Flow Velocity along Path Shown in Fig. 11, for Different Instants in Time of September 14, 1993 Rio Missiaga Event

with U = mean flow velocity and Y = flow depth, playing for the diffusion-convection equation, (20), the same role as the Reynolds number ($R = 4UY/\nu$, where ν is the kinematic viscosity) plays for the momentum equation, as a measure of the ratio of the convective flux to the diffusive flux. For very high

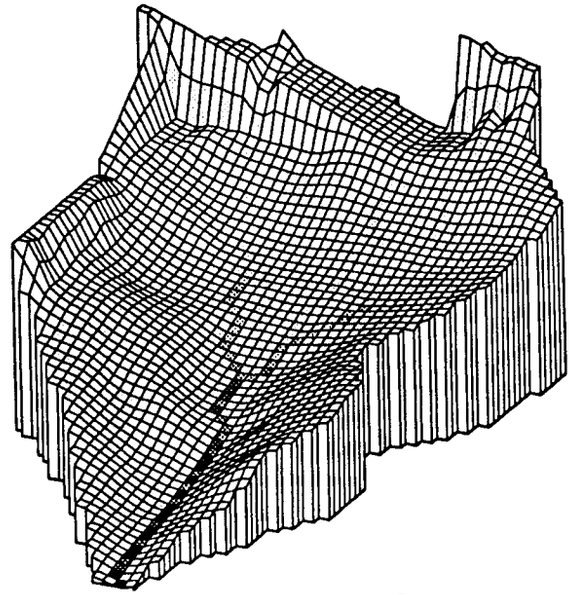

FIG. 16. Map of Hydraulic Diffusivities $\tilde{D}_h$ over Rio Missiaga Catchment (See Table 2), as Obtained from Eq. (38) in Which q_r = 10 mm h^{-1}; Darker Shades Represent Higher Diffusivities: $\tilde{D}_h$ Ranges from 0 to 1.93 m^2 s^{-1} with Average Value of 4.86 × 10^{-2} m^2 s^{-1}

values of Péclet number, (20) will be mostly of a convective nature. From (36) and (24) the Péclet number can be expressed as

$$\tilde{P}e = 8S_0/\cos\beta \tag{37}$$

Although the steeply sloping Rio Missiaga catchment is characterized predominantly by convection rather than diffusion, the variability of hydraulic diffusivity of surface flows in response to a hypothetical rainfall excess forcing of intensity q_r = 10 mm h^{-1} and duration greater than the time of concentration of the basin

$$\tilde{D}_h = \frac{3q_r^{1-b'}A_o^{b''-b'}\cos\beta}{2(3+2b')B_{ro}Q_{ro}^{-b'}S_0}A^{1-b''} \tag{38}$$

is plotted in Fig. 16 to show how the application of the Muskingum-Cunge scheme to the considered channel network is capable of distinguishing hillslope areas, where convection is the predominant physical mechanism, and lowland areas, where physical damping may be important. Comparison of Figs. 1 and 16 emphasizes how the model can automatically identify catchment areas characterized by different dynamics. The kinematic wave description applies for steeply sloping hillslopes, while the diffusion-convection wave description applies in lowland areas, where the conditions of slope and flow depth make physical damping an important effect.

SUMMARY AND CONCLUSIONS

The Muskingum-Cunge routing scheme with variable parameters was applied to DEM-based conceptual transport networks in order to describe distributed catchment dynamics in response to storm events. Each elemental channel of the network has bed slope that depends on the DEM cell location, and cross-section width that is allowed to vary dynamically according to the Leopold and Maddock (1953) at-a-station and downstream relationships. Overland and channel flow is assumed to occur in those cells for which the upstream drainage area A is less or greater than a given threshold value A^*, respectively. The appraent Gauckler-Strickler roughness coefficient is assumed as an overall distributed parameter to describe

the different processes that characterize overland and channel flow.

Numerical experiments were performed using hypothetical hillslopes in order to test mass conservation and accuracy of the method for possible slope and roughness configurations that may occur in a natural catchment. Errors in mass balance did not exceed 2%. Numerical experiments indicate that accuracy is preserved for a wide range of slope and roughness characteristics, space-time resolutions, and rainfall excess forcing rates. Fluctuations in discharge may occur in response to discontinuities in rainfall excess representation if the Courant number Cu exceeds a threshold of about 3. However, model application to Rio Missiaga catchment shows these fluctuations to be dampened when propagating downstream, so that accuracy is generally preserved for catchment scale simulations, and also for computationally inexpensive space-time discretizations (Δx = 50 m, Δt = 1/12 h), for which $Cu > 3$ may occur.

The combined use of the DEM-derived transport network structure, of the scaling concept for hydraulic geometry of channels, and of the diffusion wave equations for both overland and channel flow can help in investigating the nonlinear dynamics of basin response to storm rainfall, where basin topography and stream channel geometry play an important role. Computational experience indicates this approach as an efficient alternative to the Saint-Venant equations in modeling surface runoff in natural basins, where these equations could be hardly applied due to insufficient detail in the knowledge of boundary conditions. Further theoretical work and field inspections are suggested to investigate the representation of hydraulic geometry of reaches in natural drainage systems, especially at the mid- and large-size catchment scales.

ACKNOWLEDGMENTS

This research was jointly supported by the Ministero dell'Università e della Ricerca Scientifica e Tecnologica of Italy through the grant MURST 40% Processi Idrologici Fondamentali, and by the Gruppo Nazionale per la Difesa dalle Catastrofi Idrogeologiche, contribution 95.00273.PF42. Vigilio Villi (CNR, Padova, Italy) is gratefully acknowledged for providing data for the Rio Missiaga catchment. Discussions with Paolo La Barbera (Università degli Studi di Genova, Italy), Marco Mancini (Politecnico di Milano, Italy), and Claudio Paniconi (CRS4, Cagliari, Italy) are acknowledged and appreciated. The writers thank the anonymous reviewers for their helpful comments.

APPENDIX I. CHARACTERISTICS OF FLOW IN WIDE RECTANGULAR CHANNELS WITH DYNAMICALLY VARIABLE WIDTH

The Manning-Gauckler-Strickler equation for wide channels with rectangular cross section

$$Q = Bk_S S_f^{1/2} Y^{5/3} \tag{39}$$

where Q = discharge; B = flow width; k_S = apparent Gauckler-Strickler roughness coefficient; S_f = friction slope; and Y = flow depth, can be generalized to the case in which the flow width varies with discharge by incorporating (10) into (39). If one considers the obtained equation

$$Y = \mathcal{B}^{-3/5} k_S^{-3/5} S_f^{-3/10} Q^{3/5(1-b')} \tag{40}$$

and (10) to express the flow area $\Omega = BY$, one can solve for Q to obtain the generalized friction (21). The kinematic wave celerity $c_k = dQ/d\Omega$ given in (23) is directly derived from (21).

The hydraulic diffusivity D_h in (20) is derived from the continuity equation and a simplified momentum equation

$$\frac{\partial Q}{\partial s} + \frac{\partial \Omega}{\partial t} = q_L; \quad \frac{\partial (Y \cos \beta)}{\partial s} = S_0 - S_f \tag{41,42}$$

where Q = discharge; $\Omega = BY$ = flow area; B and Y = flow width and depth; s and t = spatial and temporal coordinates; q_L = lateral inflow; β = channel bed inclination angle; S_0 = sin β = channel bed slope; and S_f = friction slope (Hayami 1951). Since $B = B[Q, (Y)]$, (41) can be written in the form

$$\frac{\partial Q}{\partial s} + B^* \frac{\partial Y}{\partial t} = q_L \tag{43}$$

where it has been defined that

$$B^* = B + Y \frac{\partial B}{\partial Y} \tag{44}$$

Eqs. (43) and (42) can be coupled into a single equation by deriving the first with respect to s and the second with respect to t in order to eliminate the mixed derivative $\partial^2 Y/(\partial s \partial t)$. On applying the equations

$$\frac{\partial S_f}{\partial t} = \frac{\partial S_f}{\partial Q} \frac{\partial Q}{\partial t} + \frac{\partial S_f}{\partial Y} \frac{\partial Y}{\partial t} \tag{45}$$

and, from (43)

$$\frac{\partial Y}{\partial t} = \frac{1}{B^*} \left(q_L - \frac{\partial Q}{\partial s} \right) \tag{46}$$

one obtains

$$\frac{\partial^2 Q}{\partial s^2} = \frac{1}{D_h} \left[\frac{\partial Q}{\partial t} - \tilde{c}_k \left(q_L - \frac{\partial Q}{\partial s} \right) \right] + \frac{\partial q_L}{\partial s} \tag{47}$$

where

$$\tilde{c}_k = -\frac{1}{B^*} \left(\frac{\partial S_f}{\partial Y} - \frac{\cos \beta}{B^*} \frac{\partial B^*}{\partial s} \right) \Big/ \frac{\partial S_f}{\partial Q} \tag{48}$$

and

$$D_h = 1 \Big/ \left(\frac{B^*}{\cos \beta} \frac{\partial S_f}{\partial Q} \right) \tag{49}$$

The wave celerity $\tilde{c}_k$ can be expressed as sum $\tilde{c}_k = \tilde{c}_k' + \tilde{c}_k''$, where

$$\tilde{c}_k' = -\frac{1}{B^*} \frac{\partial S_f}{\partial Y} \Big/ \frac{\partial S_f}{\partial Q} \tag{50}$$

and

$$\tilde{c}_k'' = \frac{\cos \beta}{B^{*2}} \frac{\partial B^*}{\partial Q} \Big/ \frac{\partial S_f}{\partial Q} \frac{\partial Q}{\partial s} \tag{51}$$

One obtains

$$\tilde{c}_k' = 5/(3 + 2b') \mathcal{B}^{-2/5} k_S^{3/5} S_0^{3/10} Q^{2/5(1-b')} \tag{52}$$

$$\tilde{c}_k'' = \frac{3b' \cos \beta}{2(3 + 2b') S_0 \mathcal{B} Q^{b'}} \frac{\partial Q}{\partial s} \tag{53}$$

and (24) for D_h. From computational results, $\tilde{c}_k'' << \tilde{c}_k'$ and thus, neglecting $\tilde{c}_k''$, $\tilde{c}_k$ equals the kinematic celerity c_k given by (23).

APPENDIX II. DIFFUSION WAVE FORMULATION FOR SUBSURFACE STORMFLOW

To incorporate the rapid subsurface storm-flow response of the catchment [see Beven (1981)], a diffusion wave model similar to the model described earlier is applied. Local contributions to subsurface runoff that result from the soil water balance model described in Orlandini et al. (in press, 1996) are routed on a conceptual transport network extracted from DEM data. Wave celerity and diffusivity are estimated by incorporating Darcy's law into the model instead of the Manning-Gauckler-Strickler equation. Subsurface wave celerity is

described by applying the kinematic wave approximation of saturated subsurface flow and assuming that the hydraulic gradient equals the topographic slope S_0. From the flow equation

$$Q^+ = \Omega^+ K_h S_0 \tag{54}$$

where Q^+ = subsurface storm-flow discharge; Ω^+ = apparent flow area; and K_h = hydraulic conductivity in a direction parallel to the flow, one obtains

$$c_k^+ = K_h S_0 / \theta_s \tag{55}$$

and

$$D_h^+ = Q^+ / (\theta_s B^+ S_0) \tag{56}$$

where c_k^+ and D_h^+ = kinematic wave celerity and diffusivity of subsurface stormflow; θ_s = soil porosity; and B^+ = flow width.

High hydraulic conductivities are indicated by the small response times of many catchments to subsurface flow, particularly forested catchments [see Mosley (1979), Sloan and Moore (1984)]. This may be due to water flowing through interconnected macropores created by roots, other organic matter, and cracks between aggregates and rocks rather than through the soil matrix. Hence the soil porosity θ_s and hydraulic conductivity K_h used to characterize the subsurface flow may be different from those measured from small soil cores. For fields application of the model, θ_s and K_h should be considered as effective parameters of the soil profile rather than being derived from the measured values of soil porosity and hydraulic conductivity for the soil matrix [see Moore and Grayson (1991)].

APPENDIX III. REFERENCES

Agnese, C., D'Asaro, F., and Giordano, G. (1988). "Estimation of the time scale of the geomorphologic instantaneous unit hydrograph from effective streamflow velocity." *Water Resour. Res.*, 24(7), 969–978.

Band, L. E. (1986). "Topographic partition of watersheds with digital elevation models." *Water Resour. Res.*, 22(1), 15–24.

Bathurst, J. C. (1986). "Physically-based distributed modelling of an upland catchment using the Système Hydrologique Européen." *J. Hydro.*, Amsterdam, The Netherlands, Vol. 87, 79–102.

Beven, K. (1981). "Kinematic subsurface stormflow." *Water Resour. Res.*, 17(5), 1419–1424.

Beven, K. J., and O'Connell, P. E. (1982). "On the role of distributed models in hydrology." *Rep. 81*, Inst. of Hydro., Wallingford, England.

Brandford, G. E., and Meadows, M. E. (1990). "Finite element simulation of nonlinear kinematic surface runoff." *J. Hydro.*, Amsterdam, The Netherlands, 119, 335–356.

Bras, R. L. (1990). *Hydrology: an introduction to hydrologic science.* Addison-Wesley, Reading, Mass.

Carlston, C. W. (1969). "Downstream variations in the hydraulic geometry of streams: special emphasis on mean velocity." *Am. J. Sci.*, Vol. 267, 499–509.

Cunge, J. A. (1969). "On the subject of a flood propagation computation method (Muskingum method)." *J. Hydr. Res.*, 7(2), 205–230.

Emmett, W. W. (1978). "Overland flow." *Hillslope hydrology*, M. J. Kirkby, ed., John Wiley & Sons, Inc., New York, N.Y., 145–176.

Friz, C., Gatto, G., Villi, V., and Caleffa, G. (1983). "Groundwater resources of a typical catchment in the Dolomites area: The Rio Missiaga Catchment (Belluno, Italy)." *Memorie Scienze Geologiche*, Vol. 36, 293–315 (in Italian).

Hayami, S. (1951). "On the propagation of flood waves." *Disaster Prevention Res. Inst. Bull. 1*, Kyoto, Japan.

Julien, P. Y., Saghafian, B., and Ogden, F. L. (1995). "Raster-based hydrologic modeling of spatially-varied surface runoff." *Water Resour. Bull.*, 31(3), 523–536.

Kibler, D. F., and Woolhiser, D. A. (1972). "Mathematical properties of the kinematic cascade." *J. Hydro.*, Amsterdam, The Netherlands, Vol. 15, 131–147.

Kouwen, N., and Li, R. M. (1980). "Biomechanics of vegetative channel linings." *J. Hydr. Div.*, ASCE, Vol. 106, 1085–1103.

Leopold, L. B., and Maddock Jr., T. (1953). "The hydraulic geometry of steam channels and some physiographic implications." *Profl. Paper 252*, U.S. Geol. Surv., Washington, D.C.

Leopold, L. B., Wolman, M. G., and Miller, J. P. (1964). *Fluvial processes in geomorphology.* W. H. Freeman, San Francisco, Calif.

Li, R. M., Ponce, V. M., and Simons, D. B. (1980). "Modeling rill density." *J. Irrig. and Drain. Div.*, ASCE, 106(1), 63–67.

Montgomery, D. R., and Foufoula-Georgiou, E. (1993). "Channel network source representation using digital elevation models." *Water Resour. Res.*, 29(12), 3925–3934.

Moore, I. D., and Grayson, R. B. (1991). "Terrain-based catchment partitioning and runoff prediction using vector elevation data." *Water Resour. Res.*, 27(6), 1177–1191.

Mosley, M. P. (1979). "Streamflow generation in a forested watershed, New Zealand." *Water Resour. Res.*, 15(4), 795–806.

Natural Environment Research Council (NERC). (1975). *Flood Studies Rep.*, Flood Routing Studies III, Inst. of Hydro., Wallingford, England.

Newson, M. D., and Harrison, J. G. (1978). "Channel studies in the Plynlimon experimental catchments." *Rep. 47*, Inst. of Hydro., Wallingford, England.

Orlandini, S. (1995). "Space-time dependence of catchment-scale hydrologic processes: comparison between physically based distributed models at different levels of conceptualization," PhD thesis, DIIAR, Politecnico di Milano, Milano, Italy (in Italian).

Pilgrim, D. H. (1977). "Isochrones of travel time and distribution of flood storage from a tracer study on a small watershed." *Water Resour. Res.*, 13(3), 587–595.

Ponce, V. M. (1986). "Diffusion wave modeling of catchment dynamics." *J. Hydr. Engrg.*, ASCE, 112(8), 716–727.

Ponce, V. M., and Theurer, F. D. (1982). "Accuracy criteria in diffusion routing." *J. Hydr. Div.*, ASCE, 108(6), 747–757.

Ponce, V. M., and Yevjevich, V. (1978). "Muskingum-Cunge method with variable parameters." *J. Hydr. Div.*, ASCE, 104(12), 1663–1667.

Rinaldo, A., Marani, A., and Rigon, R. (1991). "Geomorphological dispersion." *Water Resour. Res.*, 27(4), 513–525.

Ross, B. B., Contractor, D. N., and Shanholtz, V. (1979). "A finite element model of overland flow and channel flow for assessing the hydrologic impact of land-use change." *J. Hydro.*, Amsterdam, The Netherlands, 41, 11–30.

Sloan, P. G., and Moore, I. D. (1984). "Modelling subsurface stormflow on steeply sloping forested watersheds." *Water Resour. Res.*, 20(12), 1815–1822.

Szymkiewicz, R. (1991). "Finite element method for the solution of the Saint Venant equations in an open channel network." *J. Hydro.*, Amsterdam, The Netherlands, Vol. 122, 275–287.

Wooding, R. A. (1966a). "A hydraulic model for the catchment-stream problem. I: Kinematic wave theory." *J. Hydro.*, Amsterdam, The Netherlands, Vol. 3, 254–267.

Wooding, R. A. (1966b). "A hydraulic model for the catchment-stream problem. II: Numerical solutions." *J. Hydro.*, Amsterdam, The Netherlands, Vol. 3, 268–282.

Wooding, R. A. (1966c). "A hydraulic model for the catchment-stream problem. III: Comparison with runoff observation." *J. Hydro.*, Amsterdam, The Netherlands, Vol. 4, 21–37.

APPENDIX IV. NOTATION

The following symbols are used in this paper:

A = upstream drainage area;
A_o = catchment drainage area;
A^* = threshold drainage area;
a' = coefficient of "at-a-station" width-discharge relationship, Eq. (1);
a'' = coefficient of "downstream" width-discharge relationship, Eq. (2);
B = channel width;
B_r = reference value of channel width at-a-station, for discharge Q_r;
B_{ro} = reference value of channel width at the catchment outlet, for discharge Q_{ro};
b' = exponent of at-a-station width-discharge relationship, Eq. (1);
b'' = exponent of downstream width-discharge relationship, Eq. (2);
Cu = Courant number, $Cu = ck\Delta t/\Delta s$;
c_k = kinematic wave celerity, $c_k = dQ/d\Omega$;
c_k^+ = kinematic wave celerity for subsurface flow;
D = cell Reynolds number, $D = 1 - 2X$;
D_h = hydraulic diffusivity, $D_h = Q/(2BS_0)$;
D_h^+ = hydraulic diffusivity for subsurface flow;
D_n = numerical diffusion coefficient, $D_n = c_k\Delta s(1/2 - X)$;

i = spatial discretization index;
j = temporal discretization index;
k_S = Gauckler-Strickler roughness coefficient ($k_S = 1/n$);
n = Manning roughness coefficient ($n = 1/k_S$);
Pe = Péclet number, $Pe = 4UY/D_h$;
Q = surface flow rate, discharge;
Q^+ = subsurface flow rate;
Q_r = reference value for discharge at-a-station;
Q_{ro} = reference value for discharge at the catchment outlet;
$\bar{Q}$ = three-point average discharge in the computational cell;
q = rainfall excess rate, per unit of catchment area;
q_r = reference value for rainfall excess rate, $q_r = Q_r/A$;
q_L = lateral inflow rate, per unit of channel length;
S_f = friction slope;
S_0 = channel bed slope;
s = spatial coordinate, along channel;
R = Reynolds number, $R = 4UY/v$;
T = simulation time period;
t = time variable;
V_Q = cumulative volume of outlet discharge;
V_q = cumulative volume of rainfall excess;
X = Muskingum-Cunge weighting factor;
x = horizontal space coordinate;
Y = flow depth;
y = horizontal space coordinate;
Δs = space interval, along channel;
Δt = time interval;
Δx = DEM cell size in the x-direction;
Δy = DEM cell size in the y-direction;
ε_M = relative error in mass balance;
θ_s = soil porosity; and
Ω = flow area.